ARQII Publication
http://arqiipubl.com/ams
APPLICATIONS OF
MODELLING AND SIMULATION
eISSN 2600-8084
VOL 6, 2022, 64-71

FEM of Air-Coupled Circular Capacitive Micromachined Ultrasonic Transducer for Anodic Bonding Process using SOI Wafer

Gurpreet Singh Gill[1,2*], Sanjay Kumar[1,3], Ravindra Mukhiya[1] and Vinod Kumar Khanna[1,4]

[1]CSIR - Central Electronics Engineering Research Institute (CEERI), Pilani-333031(Rajasthan), India
[2]The University of Western Australia, Australia
[3]Indian Institute of Technology Indore, India
[4]Retired from CSIR - CEERI, Pilani-333031(Rajasthan), India

[*]Corresponding author: er.gsgill@gmail.com

Submitted 22 March 2022, Revised 03 May 2022, Accepted 12 May 2022, Available online 13 June 2022.

Abstract: In this paper, Finite Element Method (FEM)-based design and simulation of circular capacitive micromachined ultrasonic transducer (CMUT) has been discussed. The FEM simulation of CMUT is accomplished by using MEMCAD tools CoventorWare® and COMSOL™. The simulation has been performed for air-coupled CMUT devices in which the resonance frequency of the designed CMUT device is 3.9 MHz. Moreover, the simulation results for resonance frequency and pull-in voltage show good agreement with analytical calculations. Finally, a device layer transfer fabrication process flow is also proposed to develop the MEMS-based CMUT devices.

Keywords: CMUT; FEM modelling; Pull-in voltage; Resonance frequency; Wafer bonding.

1. INTRODUCTION

Ultrasonic waves ranging from 2-18 MHz are commonly used for ultrasound image application, and generated by ultrasonic transducers [1]. Nowadays, Micro-Electro-Mechanical System (MEMS) based Capacitive Micromachined Ultrasonic Transducers (CMUTs) are used for this purpose. The piezoelectric transducers have been used for medical imaging applications during the last 50 years. However, due to impedance mismatching with air, self-heating, high dielectric losses at high frequencies and austere geometric tolerances in the piezoelectric transducers, this technology has taken a stride towards the capacitive transducers [2–7] for medical imaging and therapeutic applications. The basic principle of operation is based on the thin film vibrations when subjected to an electrostatic force for generating and sensing sonic waves [6]. The vacuum-sealed and unsealed devices are developed for this operation, ranging in radius from a few microns to several hundred microns [2, 6]. CMUTs are generally fabricated using the sacrificial release method and wafer bonding technique. In the case of the standard sacrificial release method, the membrane is released by using MEMS surface micromachining techniques while bonding techniques for instance anodic bonding, fusion bonding, and adhesive bonding, are generally used for the fabrication of pressure sensors and accelerometers. For achieving high membrane uniformity, the wafer-bonding technique is highly recommended, although, it is a bulky process [8].

This paper summarizes the comparative study of analytical and simulation results for the circular CMUT device to be realized by the anodic wafer bonding technique using the silicon-on-insulator (SOI) wafer. The operation modes and device descriptions of CMUT are presented in Section 2. In Section 3, the mathematical analysis is discussed. The simulation study is revealed in Section 4. Moreover, the results and discussion part are delineated in Section 5. Section 6 describes the fabrication process flow used in CMUT device fabrication via anodic bonding process and finally, conclusions are drawn in Section 7.

2. DEVICE DESCRIPTION

The capacitive micromachined ultrasonic transducers are used for generating ultrasound frequency in the range of several Mega-Hertz. The working principle is based on the “electrostatic” phenomena. Typically, the capacitive micromachined ultrasonic transducers are operated in two modes: transmitter mode and receiver mode. In the transmitter mode, DC voltage is applied between the top and bottom electrodes, and due to the applied DC potential, the electrostatic force is generated, and

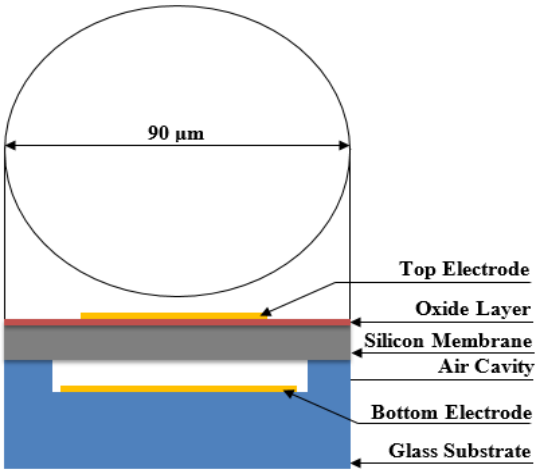

Figure 1. Cross-sectional schematic of a proposed CMUT single-cell structure with 90 μm diameter of suspended membrane. Detailed information on layers thickness is explained in Table 1

Table 1. Design shape, parameters, materials and dimensions for all the layers selected for the analytical and simulation study of CMUT

Parameters	Dimension/Materials
Base material	Silicon and Pyrex
Membrane material	Silicon and Silicon dioxide
Shape of the membrane	Circular
Size of the membrane	90 μm (Diameter)
Thickness of the membrane	2 μm Si and 1 μm SiO_2
Air cavity height	0.3 μm
Top/bottom electrode	Ti/Cr + Gold
Electrode thickness	220 nm

the membrane deflects towards the bottom electrode. After that, an AC signal of frequency, which is equivalent to the first mode of the natural frequency of the membrane, is superimposed on the DC voltage. Ultrasonic waves are generated with respect to applied AC signal frequency. In the receiver mode, the ultrasonic waves impinge on the membrane, and correspondingly the membrane is deflected. In this case, the applied DC potential is fixed and the membrane vibrates due to applied ultrasonic waves [6]. Furthermore, CMUTs also have two modes known as collapsed mode (pull-in) and non-collapsed mode. In the case of collapsed mode, the membrane is physically connected to the bottom electrode or substrate surface, while, in the case of non-collapsed mode, the membrane does not have any physical contact with the bottom electrode.

The representation of the proposed capacitive micromachined ultrasound transducer is revealed in Figure 1. In this structure, the bottom electrode is fixed on the Pyrex glass substrate and the top electrode is mounted on the suspended membrane. The resonance frequency of CMUT is dependent on the material properties, membrane thickness, membrane diameter, and shape of the membrane. Table 1 shows the device dimensions and parameters. Typically, a CMUT has a parallel-plate capacitor structure, the first metal electrode is fixed on the glass substrate known as the bottom electrode, and the second metal electrode is placed on a movable membrane known as the top electrode. The 0.3 μm height of the cavity is formed between the top and bottom electrodes, and titanium/chromium and gold materials are used for the top and bottom electrodes. The membrane is formed by using the SOI wafer and a cavity is formed inside the Pyrex glass [9,10].

3. MATHEMATICAL ANALYSIS

The resonance frequency response of the CMUT device depends not only upon the device parameters but also on the material properties. It is calculated by the formula given in Equation (1) and is found to be 4.1 MHz [11,12] which is close to the simulated resonance frequency i.e., 3.9 MHz.

$$f_r = \frac{0.47h}{a^2}\sqrt{\frac{E}{\rho(1-v^2)}} \tag{1}$$

It is clear from Equation (1) that the response of resonance frequency for a CMUT device is directly proportional to the thickness of the membrane (h) and Young's modulus (E) of the material. However, it is inversely proportional to the radius of the membrane (a), Poisson's ratio (v), and density of the material (ρ). For the transmission mode operation of the device, the applied DC voltage between two electrodes (top and bottom electrode), which leads to the generation of the electrostatic force between the plates of the device defined by Equation 2 [13].

$$F_{electrostatic} = \left[\frac{\pi a^2}{2(d_0-w)^2} + \frac{a}{(d_0-w)} - 1.918\right]\varepsilon_0 V^2 \tag{2}$$

where d_0 is the gap between membrane and bottom electrode, w is the distance travelled by a membrane in the z-direction, ε_0 is the dielectric permittivity of free space, and V is the applied DC voltage. Owing to this electrostatic force, the electrostatic pressure is also induced and is expressed by Equation (3).

$$P_{electrostatic} = \varepsilon_0 V^2\left[\frac{1}{2{d_0}^2} + \frac{1}{\pi a d_0} - \frac{1.918}{\pi a^2}\right] - \varepsilon_0 V^2\left[\frac{1}{{d_0}^3} + \frac{1}{\pi a {d_0}^2}\right]w_0 \tag{3}$$

To compensate for the effect of electrostatic pressure, a reverse pressure known as elastic restoring pressure is also generated inside the membrane in the direction opposite to the electrostatic pressure and is defined by Equation (4) [13].

$$P_{elastic} = \left[\frac{4\sigma h}{a^2} + \frac{64D}{a^4}\right] w_0 + \left[\frac{128\alpha D}{h^2 a^4}\right] {w_0}^3 \tag{4}$$

where $D = \tilde{E}h^3/12(1-v^2)$ is flexural rigidity, $\tilde{E} = E/(1-v^2)$ is effective Young's modulus, $\alpha = (7505 + 4250 - 2791v^2)/35280$ is an empirical parameter depending on Poisson's ratio, and σ is residual stress. In Equation (4), the first term denotes the combined stiffness due to bending and residual stress, and the second term defines the stiffness of the membrane due to non-linear stretching.

For the parallel plate actuator, the distance traveled by the diaphragm (membrane) to occur pull-in phenomena is equal to one-third of the total gap between the two plates of the actuator or the gap between the top and bottom electrode.

$$w_{0-PI} = \frac{d_0}{3} \tag{5}$$

where, '0' defines unactuated position of the membrane and PI stands for pull-in.

For getting the Equations (6) and (7), substitute Equation (5) in Equations (3) and (4), respectively

$$P_{PI-electrostatic} = \varepsilon_0 V^2 \left[\frac{1}{2{d_0}^2} + \frac{1}{\pi a d_0} - \frac{1.918}{\pi a^2}\right] - \varepsilon_0 V^2 \left[\frac{1}{{d_0}^3} + \frac{1}{\pi a {d_0}^2}\right] \frac{d_0}{3} \tag{6}$$

and

$$P_{PI-elastic} = \left[\frac{4\sigma h}{a^2} + \frac{64D}{a^4}\right] \frac{d_0}{3} + \left[\frac{128\alpha D}{h^2 a^4}\right] \left[\frac{d_0}{3}\right]^3 \tag{7}$$

It should be noted that Equations (3) and (6) are newly derived from the previously reported equations in literature by Rahman et al. [13], which were validated with physical simulation data obtained via COMSOL and CoventorWare software.

By using Equations (6) and (7), calculate the pull-in voltage for the suspended membrane. The pull-in voltage is defined as the voltage value at which the membrane collapses at the bottom electrode. The collapse voltage determined by Equation (8) is 80.09 V.

$$V_{PI} = \sqrt{\frac{\left[\frac{4\sigma h}{a^2} + \frac{64D}{a^4}\right] \frac{d_0}{3} + \left[\frac{128\alpha D}{h^2 a^4}\right] \left[\frac{d_0}{3}\right]^3}{\varepsilon_0 \left[\frac{1}{6{d_0}^2} + \frac{1}{3\pi a d_0} - \frac{1.918}{\pi a^2}\right]}} \tag{8}$$

4. FEM SIMULATION

The simulation of the CMUT has been performed using MEMCAD tools CoventorWare® and COMSOL™. The MemMech module of CoventorWare® has been used for modal analysis; and for harmonic analysis, the HarmonicEM module has been used. Figures 2 and 3 show the process flow used to create a three-dimensional (3D) model and cross-sectional view of the CMUT device using CoventorWare® and COMSOL™, respectively. The materials and their properties used during the simulation process are given in Table 2. In the whole process, the surface boundary condition has been set to "fixed all directions" [10,14]. In the case of COMSOL™, the Electromechanics interface is used to compute solid mechanics and electrostatics with a moving mesh collaboratively to model the deformation of electrostatically actuated structures. The displacements, stresses, and strains are computed using the Solid Mechanics interface, while the Electrostatics interface is used to compute the electric field, the electric displacement field, and potential distributions in dielectrics under conditions in which the electric charge distribution is explicitly prescribed. The articulation is stationary however used collectively with other physics. Additionally, the eigenfrequency, frequency-domain study, small-signal analysis, and time-domain modeling have been supported in all space dimensions.

A 65 V DC voltage has been applied as a boundary condition on the top electrode and bottom electrode set to 0 V. AC boundary condition of 6.5 V has been superimposed on DC to the top electrode. For the MemMech analysis, the same boundary condition and material property with residual stress have been used [4–6]. For the damping analysis, the DampingMM module has been used. For this purpose, tetrahedron meshing is used in all the studies. Section 5 shows all the results of circular CMUT. In the case of COMSOL™, the 75 V DC signal is applied under the terminal boundary and all the side faces are fixed; only z-direction movement is allowed. Moreover, free tetrahedral meshing is implemented to find Eigenfrequency, change in frequency, change in capacitance, and maximum displacement on applying DC voltage.

Table 2. Materials and their properties used during the simulation

Materials	Young's Modulus E (GPa)	Poisson's Ratio (v)	Density ρ (kg/m^3)
Silicon	169	0.27	2300
Silicon dioxide	70	0.17	2200
Gold	57	0.35	19300

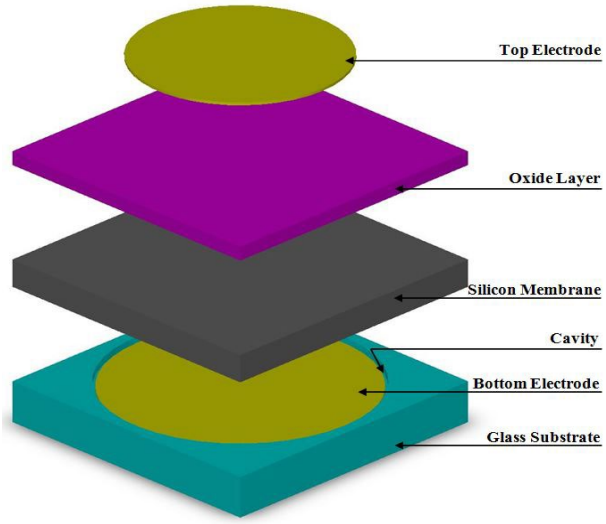

Figure 2. Process flow of circular CMUTs cell 3-D model structure using CoventorWare®

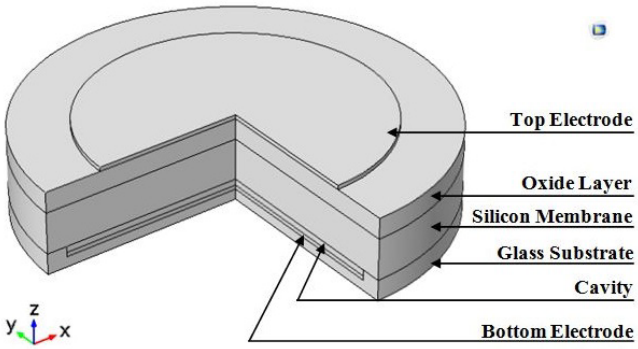

Figure 3. Cross-sectional view of CMUT cell using COMSOL™

5. RESULTS AND DISCUSSION

The simulation of the CMUT device is carried out using MEMSCAD tools, CoventorWare® and COMSOL™. Figure 4 shows the simulation results obtained using CoventorWare®. Figure 4(a) shows the modal analysis result, in which the natural frequency of the CMUT device is found to be 3.9 MHz when the surface boundary condition is set to be fixed under MemMech BCs. The maximum displacement, 9.9×10^{-5} μm, and phase shift of 90° are achieved at the resonance frequency, 3.9 MHz, on applying AC voltage with DC voltage on the electrodes, while performing the harmonic analysis using CoSolveEM settings is shown in Figures 4(b) and (c), respectively. With the electrostatic force, the membrane attains the maximum displacement at the resonance frequency. In conventional mode, the maximum deflection is accomplished by the membrane before the collapse. Figure 4(d) shows the relation between velocity and frequency, in which, when AC signal is superimposed along with DC voltage then the membrane starts to vibrate at the resonance frequency. Hence, the velocity, 1.65×10^{-11} μm/s, of the membrane is depicted at the resonance frequency. The correlation between dissipation energy and frequency is represented in Figure 4(e). Owing to the energy conversion law, when any mechanical part of the device is moving from one position to another, a small amount of energy is generated and dissipates in the form of heat. Therefore, 2.25×10^{-33} μNm energy is dissipated from the membrane on vibrations at the resonance frequency.

Figures 4(f) and (g) indicate that the value of damping coefficient is 2.39×10^{-7} N/(m/s), damping force is 5.93 N/m, and spring force is 393.68 N/m at the resonance frequency when subjected to DampingMM analysis at the atmospheric pressure. Under the effect of electrostatic force, a restoring force is generated inside the device known as a spring force. The spring force has gradually increased with frequency and at a certain value of frequency, it gets saturated. In Figure 4(h) for the transient analysis, a time-dependent study is carried out. In this case, a 65 V DC signal is applied on the top electrode and the bottom electrode is kept grounded. It is observed that the time required to reach the steady-state position for the membrane is 2.5 μs. After performing the analysis using the CoventorWare® simulation tool more analyses, for instance, biased Eigenfrequency, change in frequency, and change in capacitance with respect to applied DC voltage are computed using COMSOL™, MEMSCAD tool as shown in Figure 5.

Figure 5(a) describes the unbiased mode Eigen frequency 3.91 MHz. It is clear from Figure 5(b) the resonance frequency of the CMUT device decreases with an increase in the DC voltage owing to the spring softening effect. However, the capacitance of the device rose up with enhancing the value of applied voltage as revealed in Fig 5(d) because of the decrease of the distance between the electrodes. Moreover, the displacement of the membrane on applying the DC voltage is presented in Figures 5(c) and (e). It is also clear from the Figure 5(e) the condition for pull-in, $d_0/3$, is satisfied at 73 V. An abrupt downfall is noticed in the membrane deflection, and finally, it touches the substrate and starts operating in collapsed mode. In addition to that, the values of resonance frequency response and pull-in voltage are also calculated analytically by using Equations (1) and (8) and are found to be 4.1 MHz and 80.09 V, respectively. The relative error percentage between simulated and analytically calculated Brownian motion resonance and pull-in voltages, are <5% and <9%, respectively.

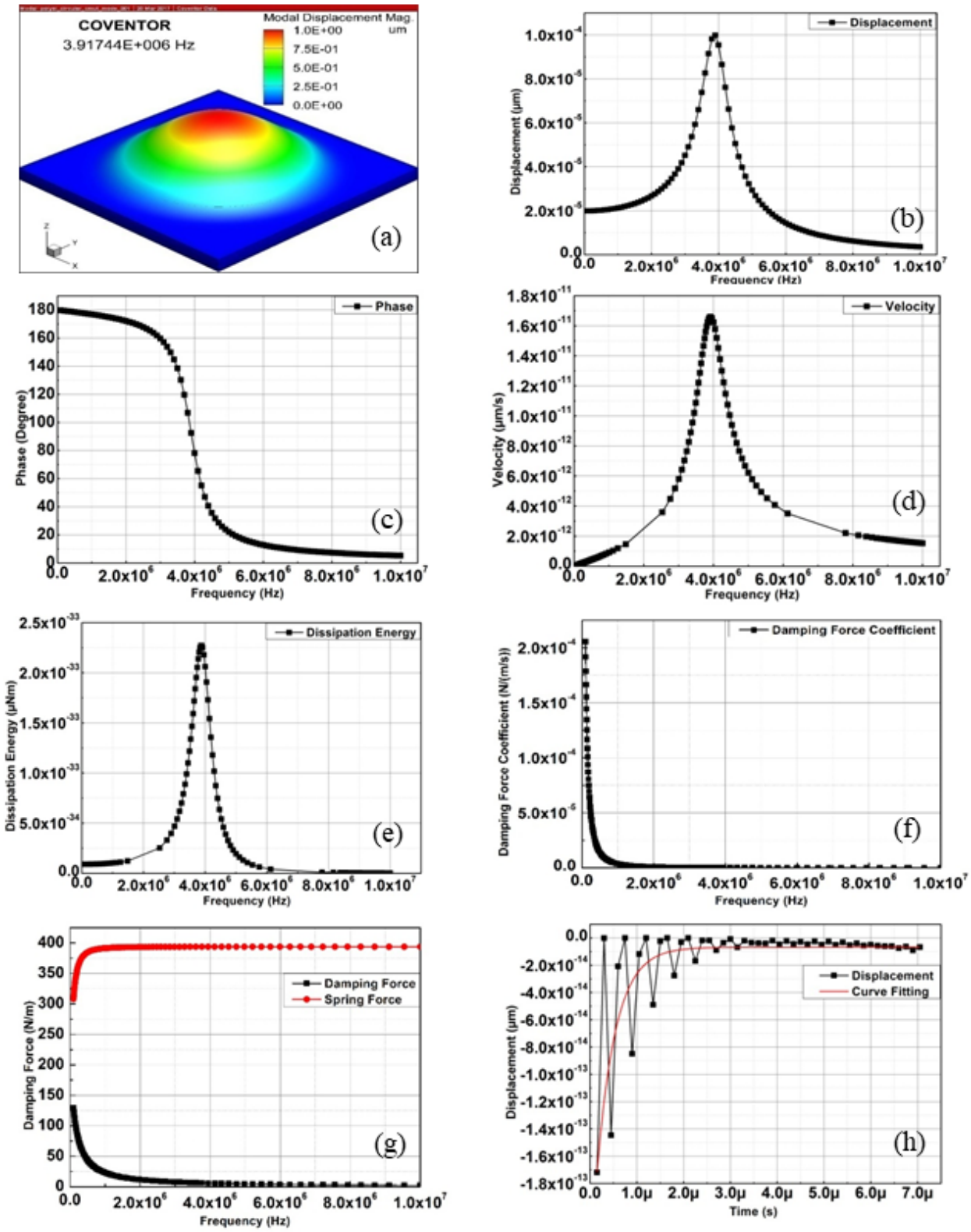

Figure 4. Various plots of circular CMUT cell using CoventorWare® tool: (a) Modal analysis; (b) Membrane displacement at resonance frequency; (c) Phase shift at resonance frequency; (d) Membrane vibration velocity at resonance frequency; (e) Energy dissipation by the membrane at resonance frequency; (f) Damping coefficient of membrane vs. frequency (g) Damping force and spring force in the membrane vs. frequency (h) Transient analysis of displacement in the membrane in order to check the settling time of membrane

6. FABRICATION PROCESS FLOW

The fabrication process flow of the complete CMUT device is shown in Figure 6 and here we have outlined the steps involved in the fabrication of the free-standing CMUT membrane are as follows:

a. A glass wafer will be selected for fabrication. The patterning of the glass wafer will be performed by spinning a photoresist on it in order to etch the air cavity inside the glass as shown in Figure 6(a).

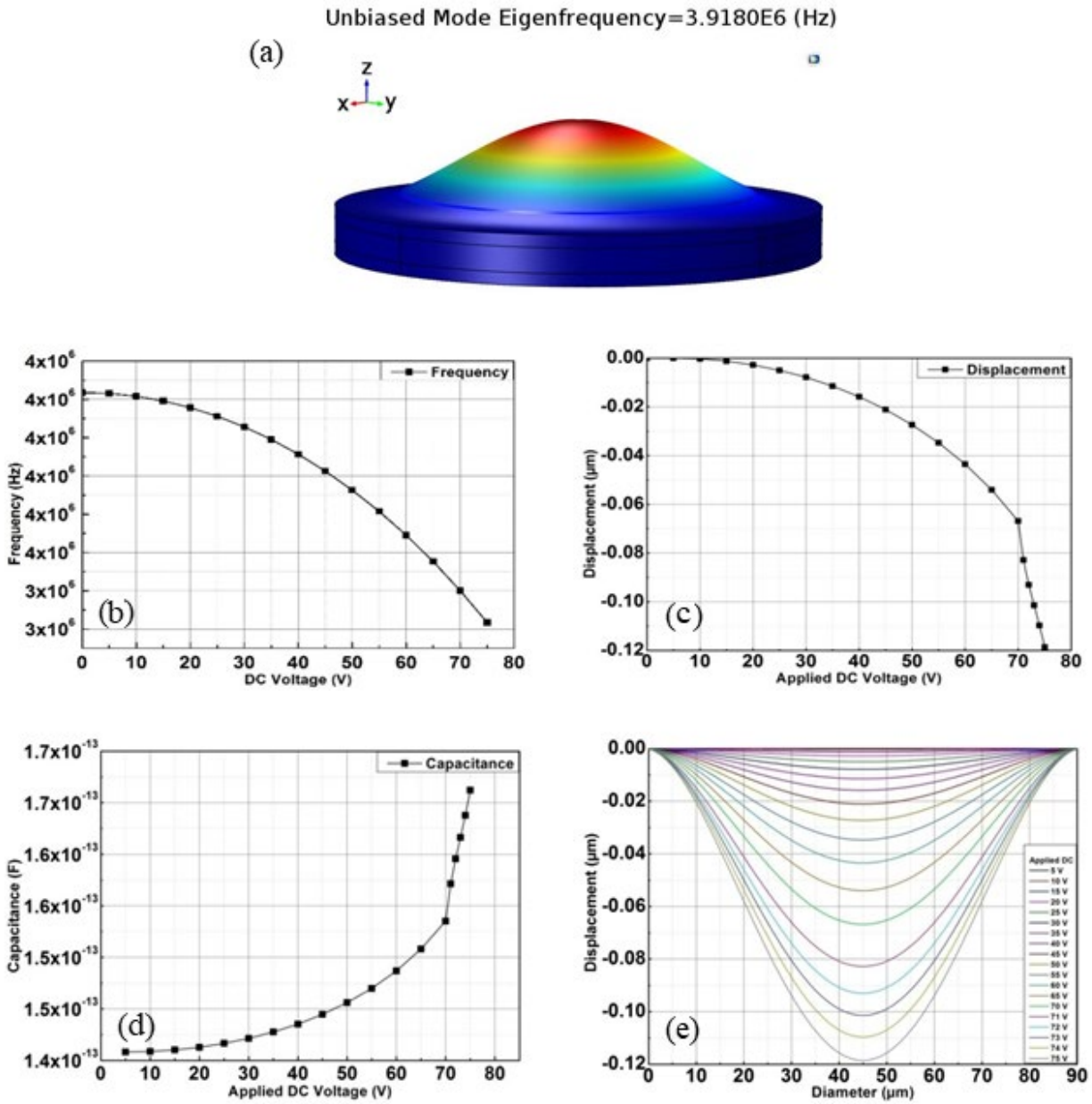

Figure 5. Various plots using COMSOL™ tool: (a) Eigenfrequency response of CMUT single cell; (b) Shift in resonance frequency along with applied DC voltage, (c) Displacement in the membrane along with applied DC voltage, (d) Increment in the capacitance of CMUT cell along with applied DC voltage, (e) Membrane displacement w.r.t different applied DC voltages i.e., pull-in analysis

b. The etching of glass will be performed with the help of buffered oxide solution, and the same photoresist mask is used for the deposition of the bottom gold electrode, as depicted in Figure 6(b), using DC sputtering technique. Figure 6(c) shows the etched glass substrate with the bottom gold electrode after the removal of unwanted gold with the help of acetone using the lift-off process.
c. Further, an SOI wafer with a 1 μm thick oxide layer and a 2 μm thick device layer will be chosen for the anodic bonding process as shown in Figure 6(d). Figure 6(e) depicts the anodic bonded SOI wafer with the glass substrate.
d. The bulk micromachining of handling silicon will be performed using an optimized Tetramethylammonium hydroxide (TMAH) process. For this, a 25% TMAH solution will be used in order to suspend the device layer over the glass substrate. However, the bulk micromachining of the silicon can be done either by dry [10,11,15] or wet micromachining technique [13,15–17]. This suspended membrane will be patterned again using a photoresist to deposit the top electrode using DC sputtering technique as illustrated in Figure 6(f). Finally, the unwanted gold is removed using the lift-off process in acetone solution as shown in Figure 6(g).

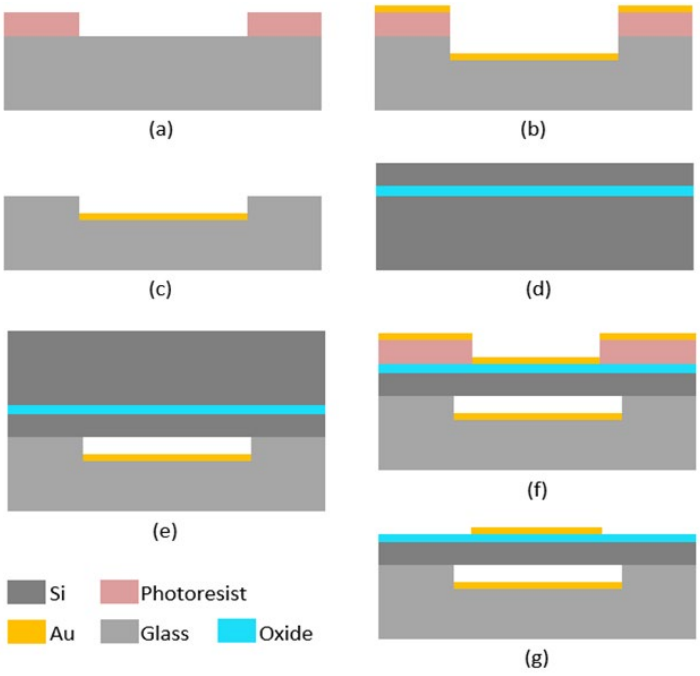

Figure 6. (a) Pyrex glass wafer coating and patterning with photoresist in order to etch the glass substrate; (b) Etching of glass substrate in buffered oxide etch (BOE) solution and deposition of the bottom gold electrode using DC sputtering technique; (c) Removal of unwanted gold using lift-off process in acetone; (d) Silicon-on-Insulator (SOI) wafer; (e) Anodic bonding of SOI wafer on the glass wafer and bulk handling silicon etched in TMAH solution; (f) Spin coating and patterning of photoresist in order to deposit top gold electrode using DC sputtering technique; and (g) Removal of unwanted gold with the help of acetone using a lift-off process

It is also important to note that the electrostatically actuated MEMS devices commonly suffer from pull-in phenomena which limit the tuning range of these devices and also lead to permanent deformation or failure of the devices. The novel anti-stiction features [18] can be incorporated in these electrostatically actuated devices to successfully recover these devices from the snap-down position and to protect them from a permanent failure.

7. CONCLUSION

In this reported work, analytical and simulation study of CMUT device has been successfully accomplished using MEMSCAD tools, CoventorWare® and COMSOL™. The simulation results are obtained by utilizing CoventorWare® and COMSOL™, which are closely matched to the analytical calculation. The simulated/calculated resonance frequency values using CoventorWare®, COMSOL™ and analytically are 3.91 MHz, 3.91 MHz, and 4.1 MHz, respectively. Similarly, the collapse voltages, 73 V and 80.09 V have been obtained using COMSOL™ and analytical calculations. Moreover, the effect of DC voltage on the membrane, resonance frequency, capacitance, and displacement are also studied. It is concluded that for the maximum efficiency in the conventional mode, the applied voltage must be below the pull-in voltage, 73 V but it should also be close to it.

ACKNOWLEDGMENT

The authors would like to express their sincere gratitude to Director, CSIR-CEERI, Pilani for his encouragement. They wish to thank all members of the Smart Sensors Group at CEERI, and Vinod Kumar Khanna is thankful to CSIR for the grant under the emeritus scientist scheme ES1314Y1514.

REFERENCES

[1] A. Carovac, F. Smajlovic and Dzelaludin Junuzovic, Application of ultrasound in medicine, *Acta Informatica Medica*, 19, 2011, 168-171.

[2] X. Jin, I. Ladabaum and B. T. Khuri-Yakub, The microfabrication of capacitive ultrasonic transducers, *Journal of Microelectromechanical Systems*, 7, 1998, 295-302.

[3] I. Ladabaum, B. T. Khuri-Yakub and D. Spoliansky, Micromachined ultrasonic transducers: 11.4 MHz transmission in air and more, *Applied Physics Letters*, 68, 1998, 7.

[4] H. T. Soh, I. Ladabaum, A. Atalar, C. F. Quate and B. T. Khuri-Yakub, Silicon micromachined ultrasonic immersion transducers, *Applied Physics Letters*, 69, 1998, 3674.

[5] A. Arora, R. Gopal, V. K. Dwivedi, C. Shekhar, B. Ahmad, Rudra Pratap and P. J. George, Fabricating capacitive micromachined ultrasonic transducers with wafer bonding technique, *Journal of Microelectromechanical Systems*, 12(2), 2003, 128-137.

[6] A. S. Ergun, G. G. Yaralioglu and B. T. Khuri-Yakub, Capacitive micromachined ultrasonic transducers: theory and technology, *Journal of Aerospace Engineering*, 16, 2003, 76-84.
[7] J. Joseph, S. G. Singh and S. R. K. Vanjari, Fabrication of SU-8 based capacitive micromachined ultrasonic transducer for low frequency therapeutic applications, *Proceedings of 37th Annual International Conference of the IEEE Engineering in Medicine and Biology Society*, Milan, Italy, 2015, 1365-1368.
[8] A. S. Erguri, Y. Huang, X. Zhuang, O. Oralkan, G. G. Yarahoglu and B. T. Khuri-Yakub, Capacitive micromachined ultrasonic transducers: fabrication technology, *IEEE Transactions on Ultrasonics, Ferroelectrics, and Frequency Control*, 52, 2005, 2242-2258.
[9] K. K. Park, H. Lee, M. Kupnik and B. T. Khuri-Yakub, Fabrication of capacitive micromachined ultrasonic transducers via local oxidation and direct wafer bonding, *Journal of Microelectromechanical Systems*, 20, 2011, 95-103.
[10] R. Mukhiya, Aditi, K. Prabakar, M. Raghuramaiah, J. Jayapandian, R. Gopal, V. K. Khanna and C. Shekhar, Fabrication of capacitive micromachined ultrasonic transducer arrays with isolation trenches using anodic wafer bonding, *IEEE Sensors Journal*, 15, 2015, 5177-5184.
[11] R. Sharma, R. Agarwal and A. A. Arora, Collapse mode characteristics of parallel plate ultrasonic transducer radiating in air and water, *Sensors & Transducers Journal*, 196, 2016, 52-56.
[12] H. Wang, X. Huang, L. Yu, Q. Ding, H. Zhang, C. He and W. Zhang, Hybrid cell structure for wideband CMUT: design method and characteristic analysis, *Micromachines*, 12(10), 2021, 1180.
[13] M. Rahman and S. Chowdhury, An accurate model for pull-in voltage of circular diaphragm capacitive micromachined ultrasonic transducers (CMUT), 2009. https://www.vlsi.uwindsor.ca/presentations/2009/An Accurate Model for Pull-in Voltage of Circular.pdf (accessed October 2, 2021).
[14] G. Gill, S. Kumar, R. Mukhiya and V. K. Khanna, FEM-based study of CMUT cell for vacuum-sealed and unsealed cavities, *3rd International Conference on Emerging Technologies: Micro to Nano*, Solapur, India, 2017.
[15] M. J. Madou, *Fundamentals of Microfabrication*, CRC Press, 2002.
[16] G. S. Gill, T. Singh and M. Prasad, Study of FBAR response with variation in active area of membrane, *AIP Conference Proceedings*, 1724, 2016, 020040.
[17] G. S. Gill and M. Prasad, Development of film bulk acoustic wave resonator: a review, *Sensor Letters*, 14(4), 2016, 346-361.
[18] G. S. Gill, M. Zawierta, D. K. Tripathi, M. Martyniuk, K. K. M. B. Dilusha Silva, G. Putrino, A. Keating and L. Faraone, Modelling and fabrication of anti-stiction features for electrostatically actuated microsystems, *Proceedings of 2018 Conference on Optoelectronic and Microelectronic Materials and Devices*, Perth, Australia, 2018, 7-10.